

Coupled-channels analyses for ${}^9,{}^{11}\text{Li} + {}^{208}\text{Pb}$ fusion reactions with multi-neutron transfer couplings

Ki-Seok Choi and Myung-Ki Cheoun*

*Department of Physics and OMEG Institute,
Soongsil University, Seoul 156-743, Korea*

W. Y. So

Department of Radiological Science, Kangwon National University at Dogye, Samcheok 245-905, Korea

K. Hagino

*Department of Physics, Tohoku University, Sendai 980-8578, Japan and
Research Center for Electron Photon Science,
Tohoku University, 1-2-1 Mikamine, Sendai 982-0826, Japan*

K. S. Kim

School of Liberal Arts and Science, Korea Aerospace University, Koyang 412-791, Korea

(Dated: November 7, 2018)

We discuss the role of two-neutron transfer processes in the fusion reaction of the ${}^9,{}^{11}\text{Li} + {}^{208}\text{Pb}$ systems. We first analyze the ${}^9\text{Li} + {}^{208}\text{Pb}$ reaction by taking into account the coupling to the ${}^7\text{Li} + {}^{210}\text{Pb}$ channel. To this end, we assume that two neutrons are directly transferred to a single effective channel in ${}^{210}\text{Pb}$ and solve the coupled-channels equations with the two channels. By adjusting the coupling strength and the effective Q -value, we successfully reproduce the experimental fusion cross sections for this system. We then analyze the ${}^{11}\text{Li} + {}^{208}\text{Pb}$ reaction in a similar manner, that is, by taking into account three effective channels with ${}^{11}\text{Li} + {}^{208}\text{Pb}$, ${}^9\text{Li} + {}^{210}\text{Pb}$, and ${}^7\text{Li} + {}^{212}\text{Pb}$ partitions. In order to take into account the halo structure of the ${}^{11}\text{Li}$ nucleus, we construct the potential between ${}^{11}\text{Li}$ and ${}^{208}\text{Pb}$ with a double folding procedure, while we employ a Wood-Saxon type potential with the global Akyüz-Winther parameters for the other channels. Our calculation indicates that the multiple two-neutron transfer process plays a crucial role in the ${}^{11}\text{Li} + {}^{208}\text{Pb}$ fusion reaction at energies around the Coulomb barrier.

PACS numbers: 24.10.-i, 25.70.Jj

Keywords: Coupled-channels method, Total fusion cross section

I. INTRODUCTION

Fusion is a process in nuclear reactions in which a projectile nucleus collides with a target nucleus and then the two nuclei are merged into a new compound nucleus. The compound nucleus formed in fusion reaction is in general highly excited, and it decays by emitting gamma ray(s), neutron(s), proton(s), and alpha particle(s). The nuclear fusion plays an important role in the energy generation in the stellar evolution as well as in the quest for superheavy elements production. See Refs. [1–5] for recent reviews.

Fusion cross sections are strongly influenced by the Coulomb barrier, which is constructed as a sum of the repulsive Coulomb and an attractive nuclear potentials. While the charge numbers of the projectile and the target nuclei provide the strength of the repulsive Coulomb potential, the mass numbers are related to the strength for the attractive nuclear potential. When the incident energy is lower than the Coulomb barrier height, most of the flux does not pass through the Coulomb barrier and is scattered elastically. In this situation, the fusion takes place only by quantum tunneling. As the incident energy increases, the fusion cross sections also increase [6], and eventually coincide with the classical fusion cross sections (see e.g., the “Wong formula” [7, 8] obtained in the parabolic approximation to the Coulomb barrier).

Recently, various radioisotope (RI) neutron-rich beams, such as ${}^6,8\text{He}$, ${}^{9,11}\text{Li}$, ${}^{11}\text{Be}$ and ${}^{16,19}\text{C}$, have been produced thanks to the remarkable advances in the radioisotope beam technology. The fusion process of such radioisotopes has attracted lots of attention. In fact, a large number of experimental works have been carried out to measure total fusion cross sections of e.g., ${}^6\text{He} + {}^{209}\text{Bi}$ [9, 10], ${}^{11}\text{Be} + {}^{209}\text{Bi}$ [11], ${}^{11}\text{Li} + {}^{208}\text{Pb}$ [12], ${}^6\text{He} + {}^{238}\text{U}$ [13], ${}^{6,8}\text{He} + {}^{197}\text{Au}$ [14], and ${}^{15}\text{C} + {}^{232}\text{Th}$ [15] systems. Many theoretical studies have also been performed by taking into account the characteristic features of weakly-bound neutron-rich nuclei, such as a halo structure and a low energy threshold for breakup processes [16–20].

In this paper, we discuss fusion reactions of the ${}^{9,11}\text{Li} + {}^{208}\text{Pb}$ systems, in which the ${}^{11}\text{Li}$ nucleus is a typical example of weakly-bound halo nuclei [21–23]. Even though the fusion of the ${}^9\text{Li}$ nucleus is considered to provide reference cross sections in discussing the fusion of the ${}^{11}\text{Li}$ nucleus, the standard coupled-channels calculations have faced difficulties in reproducing the experimental data.

*e-mail: cheoun@ssu.ac.kr (Corresponding Author)

For instance, the fusion cross sections for the ${}^9\text{Li}+{}^{70}\text{Zn}$ system are largely underestimated at energies below the Coulomb barrier even if the collective excitations in the colliding nuclei as well as the ground-state-to-ground-state two-neutron transfer channel are taken into account [24]. The fusion of the ${}^9\text{Li}+{}^{208}\text{Pb}$ system also shows a similar difficulty [12, 25]. Our first motivation in this work is to investigate whether the experimental data for the ${}^9\text{Li}+{}^{208}\text{Pb}$ system can be accounted for when one considers the two-neutron transfer to excited states, rather than to the ground state. We then discuss the fusion of the ${}^{11}\text{Li}+{}^{208}\text{Pb}$ system, which couples to the ${}^9\text{Li}+{}^{208}\text{Pb}$ system. Our second motivation in this paper is to discuss whether one can describe the fusion of ${}^{11}\text{Li}+{}^{208}\text{Pb}$ and ${}^9\text{Li}+{}^{208}\text{Pb}$ systems in a consistent manner by taking into account the multi two-neutron transfer process. One-neutron transfer is also possible process. But, for Borromean nuclei like ${}^{11}\text{Li}$, the one-neutron transfer is known to be much less probable than the two-neutron transfer, as confirmed in the data for ${}^6\text{He} + {}^{65}\text{Cu}$ system [26].

The paper is organized as follows. In Sec. II, we first analyze the fusion of the ${}^9\text{Li}+{}^{208}\text{Pb}$ system, by taking into account the two-neutron transfer channel. We then discuss the fusion of ${}^{11}\text{Li}+{}^{208}\text{Pb}$ system in Sec. III, using the result of the calculation for the ${}^9\text{Li}+{}^{208}\text{Pb}$ system. We finally summarize the paper in Sec. IV.

II. ${}^9\text{Li}+{}^{208}\text{Pb}$ FUSION REACTION

We first analyze the ${}^9\text{Li}+{}^{208}\text{Pb}$ fusion reaction. For simplicity, we ignore the effect of the collective excitations in the colliding nuclei, which is expected to be small for this system [25]. Instead, we take into account the two-neutron transfer ${}^{208}\text{Pb}({}^9\text{Li}, {}^7\text{Li}){}^{210}\text{Pb}$ channel, whose ground-state-to-ground-state Q -value is $Q_{gg} = +3.0$ MeV. An important fact is that the transfer to the ground state may not be the dominant process when the transfer Q -value is positive [27]. Rather, from the viewpoint of the Q -value matching, the transfer to excited states would be more plausible. In order to investigate the effect of such process, we here solve the coupled-channels equations [3, 28] by including the transfer channel. To this end, we follow Ref. [27] and introduce a single effective channel for the transfer partition. The resultant coupled-channels equations read,

$$\begin{pmatrix} K + V_2(r) - E & F_{2\rightarrow 3}(r) \\ F_{2\rightarrow 3}(r) & K + V_3(r) - (E + Q_{23}) \end{pmatrix} \begin{pmatrix} \psi_2(r) \\ \psi_3(r) \end{pmatrix} = 0, \quad (1)$$

where the channels 2 and 3 denote the ${}^9\text{Li}+{}^{208}\text{Pb}$ and the ${}^7\text{Li}+{}^{210}\text{Pb}$ systems, respectively. Here, K is the kinetic energy (with the centrifugal potential) and $V_i(r)$ ($i=1,2$) is the inter-nucleus potential for each partition. Q_{23} is the effective Q -value for the two-neutron transfer process, which is determined by fitting to the experimental fusion cross sections, while $F_{2\rightarrow 3}(r)$ is the coupling form

factor.

In the calculations presented below, we employ the Akyüz-Winther (AW) potential [29] for the nuclear part of $V_i(r)$, whose parameters have been globally determined. The actual values for the parameters are given in Table 1, together with the height, the position, and the curvature of the Coulomb barrier. For the coupling form factor, we use a derivative form of the Woods-Saxon potential [30], that is,

$$F_{2\rightarrow3}(r) = F_t \frac{d}{dr} \left(\frac{1}{1 + \exp((r - R_{\text{coup}})/a_{\text{coup}})} \right). \quad (2)$$

Table 1: The depth, the radius, and the diffuseness parameters for the nuclear Woods-Saxon potential for each channel in the ${}^9\text{Li} + {}^{208}\text{Pb}$ reaction. These are based on the global Akyüz-Winther (AW) potential [29]. The barrier height, V_b , the barrier position, R_b , and the barrier curvature, $\hbar\Omega$, are also shown for each potential.

Channel	V_0 (MeV)	r_0 (fm)	a_0 (fm)	V_b (MeV)	R_b (fm)	$\hbar\Omega$ (MeV)
${}^9\text{Li} + {}^{208}\text{Pb}$ (channel 2)	47.500	1.177	0.636	29.1	11.5	4.07
${}^7\text{Li} + {}^{210}\text{Pb}$ (channel 3)	47.347	1.177	0.625	29.6	11.3	4.71

Table 2: The effective transfer Q -value and the parameters for the coupling form factor given by Eq. (2), obtained by fitting the results of the coupled-channels calculations to the experimental data. Here, r_{coup} is defined as $R_{\text{coup}} = r_{\text{coup}}(A_p^{\frac{1}{3}} + A_t^{\frac{1}{3}})$, where A_p and A_t are the mass number of the projectile and the target nuclei, respectively.

Q_{23} (MeV)	F_t (MeV fm)	r_{coup} (fm)	a_{coup} (fm)
-3.204	51.367	1.357	0.264

The solid (black) line in the left panel of Fig. 1 shows the result of the two-channel calculation for fusion cross sections. In order to draw this curve, we exploit a fitting process to the experimental data and find the optimum values for the four adjustable parameters, that is, the effective Q -value, Q_{23} , and F_t , R_{coup} , and a_{coup} in the coupling form factor, Eq. (2). The optimum value for these parameters are listed in Table 2. One can see that the experimental fusion cross sections are well reproduced with this calculation. For comparison, the figure also shows the coupled-channels (CC) calculation with collective excitations in the colliding nuclei (but with no transfer coupling; the blue dotted line) as well as the single-channel calculation (the green dot-dashed line). For the former

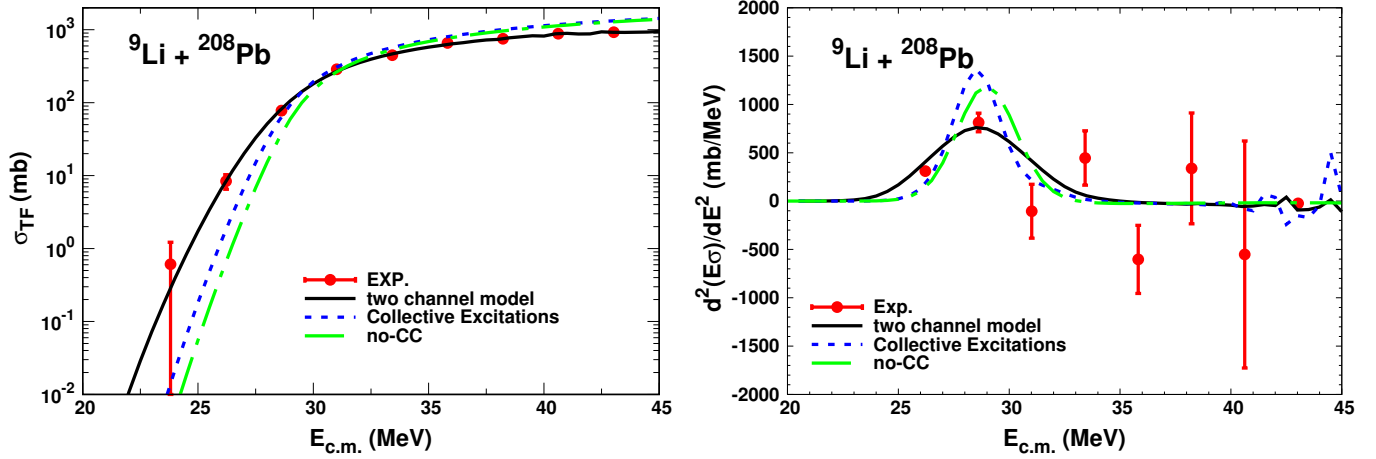


Fig. 1: (Color online) The total fusion cross sections (the left panel) and the fusion barrier distribution, $d^2(E\sigma)/dE^2$ (the right panel) for the ${}^9\text{Li} + {}^{208}\text{Pb}$ system. The black solid lines denote the results of the two-channel calculation, which takes into account the two-neutron transfer process, while the blue dashed lines are obtained by including the collective excitations in the colliding nuclei. The result of the single channel calculation is denoted by the green dot-dashed lines. See text for details. The experimental data are taken from Ref. [25].

CC calculation, we include the rotational excitation to the first excited state at 2.69 MeV in ${}^9\text{Li}$ with the quadrupole deformation parameter of $\beta_2 = 0.469$ [31] as well as the vibrational coupling to the 3_1^- state in ${}^{208}\text{Pb}$ at 2.615 MeV with the deformation parameter of $\beta_3 = 0.111$. As has been shown in Ref. [25], the collective excitations alone do not account well for the experimental data.

In the right panel of Fig. 1, we present the fusion barrier distribution defined by $d^2(E\sigma)/dE^2$ [32]. The experimental fusion barrier distribution is extracted from the experimental fusion cross sections using a point difference formula. One can see that the barrier distribution is significantly widened by the transfer coupling. This brings in the low energy strength in the barrier distribution, which eventually results in the large enhancement of subbarrier fusion cross sections shown in the left panel of Fig. 1.

III. ${}^{11}\text{Li} + {}^{208}\text{Pb}$ FUSION REACTION

We next discuss the fusion of the ${}^{11}\text{Li} + {}^{208}\text{Pb}$ system. To this end, we again neglect the collective excitations of the colliding nuclei and focus on the transfer couplings. Although the breakup of ${}^{11}\text{Li}$ would also play a role in the fusion reaction, we neglect it in the present calculation. For weakly bound nuclei, large transfer cross sections are often observed experimentally at energies below the Coulomb barrier [13, 14], and thus the role of transfer couplings is expected to be as important as the breakup channel. Since the role of transfer couplings in the fusion of weakly bound nuclei

has not been well clarified, we here concentrate on the transfer couplings, leaving the simultaneous treatment of the transfer and the breakup channels for an interesting future work.

Introducing effective transfer states as in the previous section, we thus solve the following three-channel problem:

$$\begin{pmatrix} K + V_1(r) - E & F_{1 \rightarrow 2}(r) & 0 \\ F_{1 \rightarrow 2}(r) & K + V_2(r) - (E + Q_{12}) & F_{2 \rightarrow 3}(r) \\ 0 & F_{2 \rightarrow 3}(r) & K + V_3(r) - (E + Q_{12} + Q_{23}) \end{pmatrix} \begin{pmatrix} \psi_1(r) \\ \psi_2(r) \\ \psi_3(r) \end{pmatrix} = 0, \quad (3)$$

where the channels $i=1, 2$ and 3 correspond to the $^{11}\text{Li} + ^{208}\text{Pb}$, $^9\text{Li} + ^{210}\text{Pb}$ and $^7\text{Li} + ^{212}\text{Pb}$ systems, respectively. In this equation, we have neglected the direct coupling between the channels 1 and 3, as the direct four-neutron transfer process is quite unlikely.

A. Internuclear potential for each channel

We first determine the inter-nucleus potential for each channel, $V_i(r)$, in Eq. (3). For the second and the third channels, we employ the Akyüz-Winther potential [29], as in the previous section. The actual values for the parameters are listed in Table 3. Because the mass number of the projectile and the target is different only slightly, those values are close to the parameters for the $^9\text{Li} + ^{208}\text{Pb}$ system listed in Table 1.

Table 3: Same as Table 1, but for the $^{11}\text{Li} + ^{208}\text{Pb}$ reaction. The potential for the channels 2 and 3 is based on the Akyüz-Winther potential, while the parameters for the channel 1 are obtained by fitting the double folding potential to a Woods-Saxon form.

Channel	V_0 (MeV)	r_0 (fm)	a_0 (fm)	V_b (MeV)	R_b (fm)	$\hbar\Omega$ (MeV)
$^{11}\text{Li} + ^{208}\text{Pb}$ (channel 1)	90.309	1.090	0.852	27.3	12.1	3.04
$^9\text{Li} + ^{210}\text{Pb}$ (channel 2)	47.304	1.178	0.636	29.0	11.5	4.06
$^7\text{Li} + ^{212}\text{Pb}$ (channel 3)	47.298	1.177	0.626	29.6	11.29	4.70

For the potential for the $^{11}\text{Li} + ^{208}\text{Pb}$ channel, on the other hand, one expects a large deviation from the Akyüz-Winther potential due to the halo structure of the ^{11}Li nucleus [33]. In order to take into account the halo structure, we employ a folding potential approach [34] and construct the potential as,

$$V(r) = \int d\mathbf{r}_1 \int d\mathbf{r}_2 \rho_p(r_1) \rho_t(r_2) v_{NN}(|\mathbf{r} - \mathbf{r}_1 + \mathbf{r}_2|), \quad (4)$$

where $\rho_p(r_1)$ and $\rho_t(r_2)$ are the density distribution for the projectile and target nuclei, respectively.

For the effective nucleon-nucleon interaction, v_{NN} , we here employ the M3Y interaction [35] with

the zero-range approximation to the knock-on exchange term given by

$$v_{NN}(r) = -2134 \frac{e^{-2.5r}}{2.5r} + 7999 \frac{e^{-4r}}{4r} - 275.81 \delta(\mathbf{r}), \quad (5)$$

where the value of each parameter is given in units of fm or MeV. For the density distribution for the target nucleus, we use the Woods-Saxon form,

$$\rho_t(r) = \frac{\rho_0}{1 + \exp\left(\frac{r-c}{z}\right)}, \quad (6)$$

with $c=6.67$ fm, $z=0.545$ fm and $\rho_0=0.157$ fm³ for ²⁰⁸Pb [36]. For the projectile nucleus ¹¹Li, we assume that it is comprised of a core nucleus ⁹Li and two valence neutrons due to the halo structure. The projectile density is then given by

$$\rho_p(r) = \rho_c(r) + \rho_{2n}(r), \quad (7)$$

where $\rho_c(r)$ is the core density and $\rho_{2n}(r)$ is the density for the valence neutrons. The folding potential, Eq. (4), is thus also divided into two parts,

$$V(r) = V_{c-t}(r) + V_{2n-t}(r), \quad (8)$$

with

$$V_{c-t}(r) = \int d\mathbf{r}_1 \int d\mathbf{r}_2 \rho_c(r_1) \rho_t(r_2) v_{NN}(|\mathbf{r} - \mathbf{r}_1 + \mathbf{r}_2|), \quad (9)$$

$$V_{2n-t}(r) = \int d\mathbf{r}_1 \int d\mathbf{r}_2 \rho_{2n}(r_1) \rho_t(r_2) v_{NN}(|\mathbf{r} - \mathbf{r}_1 + \mathbf{r}_2|). \quad (10)$$

In the following, we replace the interaction between the core and the target nuclei, $V_{c-t}(r)$, with the Akyüz-Winther potential for the ⁹Li+²⁰⁸Pb system. For the interaction between the valence neutrons and the target, following Ref. [34], we employ the dineutron cluster model and introduce a Yukawa function for the density of the valence neutrons, that is,

$$\rho_{2n}(s) = \rho_0 \frac{e^{-2\kappa s}}{s^2}, \quad (11)$$

where $\rho_0 = \kappa/\pi$, κ being determined from the two-neutron separation energy, $S_{2n} = 0.369$ MeV, and s is the distance between the core nucleus and the center of mass of the two valence neutrons.

The solid (black) lines in Fig. 2 show the folding potential for the ¹¹Li+²⁰⁸Pb so obtained. The left panel shows the valence-target potential, while the right panel shows the total potential, which includes the valence-target and the core-target nuclear potentials as well as the Coulomb potential between the projectile and the target nuclei.

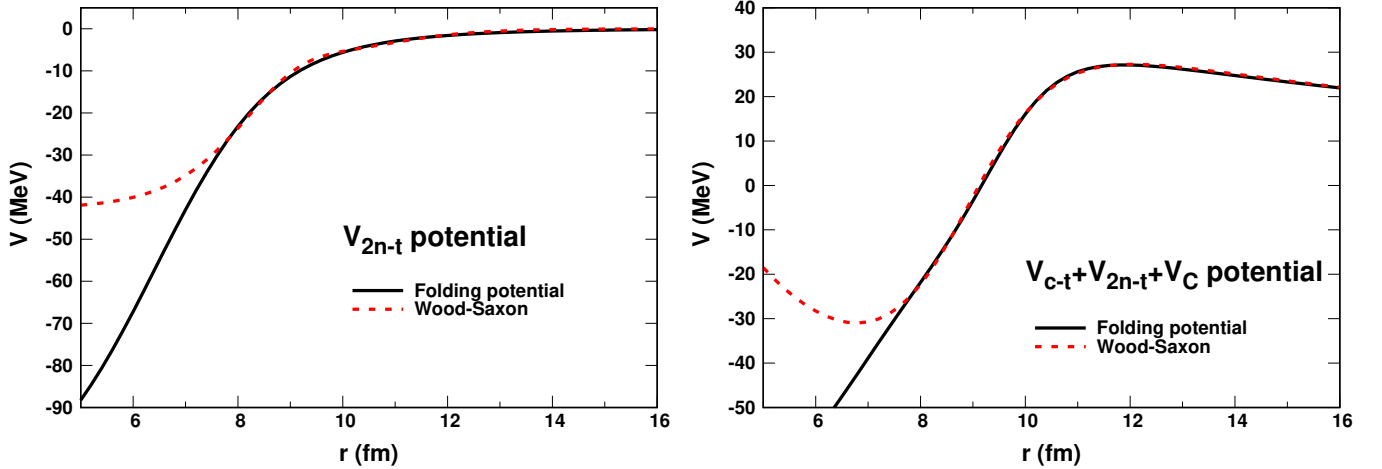


Fig. 2: (Color online) The potential for the $^{11}\text{Li} + ^{208}\text{Pb}$ fusion reaction. The left panel shows the potential between the valence neutrons in ^{11}Li and the target nucleus, while the right panel is for the total potential including the Coulomb potential. The (black) solid lines denote the folding potential, while the (red) dashed lines show its fit with a Wood-Saxon potential.

In order to discuss properties of the potential, we fit this potential with a Woods-Saxon function. The resultant potential is shown in Fig. 2 by the dashed (red) lines, whose parameters are listed in Table 3. One can see that the folding potential can be well fitted with the Woods-Saxon potential for r larger than 8 fm. Note that fusion cross sections are insensitive to the details of the nuclear potential for the smaller values of r , due to the strong absorption inside the barrier, and thus we actually use the fitted Woods-Saxon potential in the calculations presented in the next subsection.

Because of the halo structure of ^{11}Li , the potential for the $^{11}\text{Li} + ^{208}\text{Pb}$ system shows different behavior compared to the potential for the other systems. Since the Coulomb barrier is lowered, the potential is deeper than those potentials for the channels 2 and 3. Moreover, the value of diffuseness parameter, a_0 , is significantly larger, reflecting the extended density distribution of the ^{11}Li nucleus. This results in a smaller value of the barrier curvature, as shown in Table 4. We mention that this feature has been treated as a long-range interaction in Ref. [37].

B. Results of the coupled-channels calculations

Finally, we solve the coupled-channels equations, Eq. (3), and calculate fusion cross sections for the $^{11}\text{Li} + ^{208}\text{Pb}$ system. In order to reduce the number of adjustable parameters, we assume that the effective Q -value, Q_{23} , and the parameters for the transfer coupling form factor for the coupling between the channels 2 and 3 are the same as those determined in the previous section (see Table 2), even though the mass numbers are slightly different. The number of adjustable parameter is now reduced to four, that is, the effective Q -value and the parameters for the form factor for the

coupling between the channels 1 and 2. These are determined by fitting the calculated result for fusion cross sections to the experimental data, as has been done in the previous section for the ${}^9\text{Li}+{}^{208}\text{Pb}$ system. The resultant fusion cross sections are shown in the (black) solid line in the left panel of Fig. 3, whereas the resultant parameters are shown in Table 4. The theoretical uncertainties for Q and F_t for the coupling from the channel 1 to 2 are estimated to be $Q = +8.346^{+1.163}_{-0.897}$ MeV and $F_t = 40.227^{+2.45}_{-2.136}$ fm, respectively, for which we have used the χ -square fitting with the fixed values for r_{coup} and a_{coup} .

Table 4: Same as Table 2, but for the ${}^{11}\text{Li} + {}^{208}\text{Pb}$ reaction. The parameters for the coupling between the channels 1 and 2 are obtained by fitting to the experimental data, while those for the coupling between the channels 2 and 3 are taken to be the same as those in Table 2. The Q -value for the ground-state-to-ground state transfer between the channels 1 and 2 is $Q_{gg} = +8.852$ MeV.

Channel	Q (MeV)	F_t (MeV fm)	r_{coup} (fm)	a_{coup} (fm)
$1 \rightarrow 2$	+8.346	40.227	1.666	0.857
$2 \rightarrow 3$	-3.204	51.367	1.357	0.264

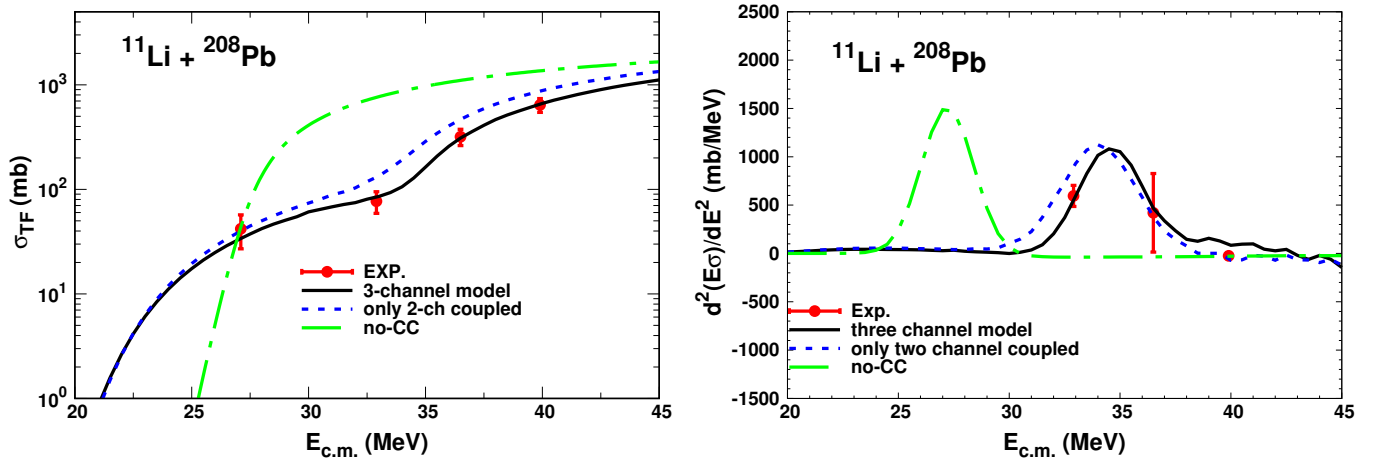


Fig. 3: (Color online) The total fusion cross sections (the left panel) and the fusion barrier distribution, $d^2(E\sigma)/dE^2$, (the right panel) for the ${}^{11}\text{Li}+{}^{208}\text{Pb}$ system. The (black) solid lines show the results of the three-channel coupling model with the ${}^{11}\text{Li}+{}^{208}\text{Pb}$, ${}^9\text{Li}+{}^{210}\text{Pb}$, and ${}^7\text{Li}+{}^{212}\text{Pb}$ channels, while the (blue) dotted lines show the result obtained by switching off the transfer coupling between ${}^9\text{Li}+{}^{210}\text{Pb}$ and ${}^7\text{Li}+{}^{212}\text{Pb}$. The (green) dot-dashed lines show the results of the single-channel calculation. The experimental data are taken from Ref. [12].

For comparison, the figure also shows the results of the single-channel calculation (the (green) dot-dashed line). One can see that the fusion cross sections are largely overestimated in this

calculation at energies above the barrier. But, if we take the neutron-transfer channel into account, they become compatible with the experimental data, as shown in the dashed (blue) line. This is due to the transfer coupling with a large positive Q -value [38, 39], for which the higher energy peak in the barrier distribution carries more weight than the lower energy peak, as is evident in the right panel in Fig. 3. The Coulomb barrier is thus effectively shifted towards high energy, reducing the fusion cross sections at energies above the barrier. At energies below the Coulomb barrier, on the other hand, fusion cross sections in the coupled-channels calculations are largely enhanced as compared to the fusion cross sections in the single-channel calculation due to the lower energy peak in the barrier distribution, even though it carries only a small weight.

In order to investigate the role of the third channel, we also present by the (blue) dotted lines the result of the two-channel calculation obtained by switching off the coupling between the channels 2 and 3. One can see that the coupling to the ${}^7\text{Li}+{}^{212}\text{Pb}$ channel, that is, the multi two-neutron transfer channel, plays a significant role, even though the main effect comes from the single two-neutron transfer channel, *i.e.*, the coupling between the channels 1 and 2.

IV. CONCLUSION

We have calculated total fusion cross sections for the ${}^9,{}^{11}\text{Li} + {}^{208}\text{Pb}$ systems, for which the ${}^{11}\text{Li}$ nucleus has a halo structure, by taking into account multiple two-neutron transfers in the coupled-channels approach. To this end, we have constructed the nuclear potential for the ${}^{11}\text{Li} + {}^{208}\text{Pb}$ channel with the double folding procedure based on the dineutron cluster model. We have employed the global Aküz-Winther potential for all the other channels. By adjusting the effective transfer Q -values and the parameters for the coupling form factors, we have successfully reproduced the experimental fusion cross sections for both the systems simultaneously. This clearly indicates that (multi-) neutron transfer channels owing to the positive Q value, specifically for ${}^{11}\text{Li}$ channel, play an important role in fusion of weakly bound nuclei. We did not include the breakup channel in this work since we expected that the breakup channel does not affect much cross-sections for total fusion at energies above the Coulomb barrier owing to the large gap between the Coulomb barrier and the breakup channel Q value.

For fusion of the ${}^{11}\text{Li} + {}^{208}\text{Pb}$ system, the experimental data exist only at four energy points. This has prevented us to uniquely determine the parameters, especially the effective Q -values for the transfer couplings. In order to gain a deeper insight into the role of transfer couplings in fusion of weakly bound nuclei, it would be helpful if total fusion cross sections for this system will be measured in near future at more data points, especially at energies below the Coulomb barrier.

ACKNOWLEDGMENT

This work was supported by the National Research Foundation of Korea (Grant Nos. NRF-2016R1C1B1012874, NRF-2014R1A1A2A16052632, NRF-2015R1D1A3A01017378, NRF-2015R1A2A2A01004727, NRF-2015K2A9A1A06046598, and NRF-2017R1E1A1A01074023). K.H. thanks Soongsil University and Kangwon National University at Dogye for their hospitality and for financial supports for his visit to those universities.

- [1] A.B. Balantekin and N. Takigawa, *Rev. Mod. Phys.* **70**, 77 (1998).
- [2] M. Dasgupta, D.J. Hinde, N. Rowley, and A.M. Stefanini, *Annu. Rev. Nucl. Part. Sci.* **48**, 401 (1998).
- [3] K. Hagino and N. Takigawa, *Prog. Theor. Phys.* **128**, 1061 (2012).
- [4] B.B. Back, H. Esbensen, C.L. Jiang, and K.E. Rehm, *Rev. Mod. Phys.* **86**, 317 (2014).
- [5] G. Montagnoli and A.M. Stefanini, *Eur. Phys. J.* **A53**, 169 (2017).
- [6] W. So, *J. Korean. Phys. Soc.* **59**, 2869 (2011).
- [7] C. Y. Wong, *Phys. Rev. Lett.* **31**, 766 (1973).
- [8] N. Rowley and K. Hagino, *Phys. Rev. C* **91**, 044617 (2015).
- [9] J.J. Kolata *et al.*, *Phys. Rev. Lett.* **81**, 4580 (1998).
- [10] A. A. Hassan, S. Lukyanov, R. Kalpakchieva, Yu. E. Penionzhkevich, R. A. A. stabyan, J. Vinsour, Z. Dlouhy, A. A. Kulko, J. Mrazek, S. P. Lobastov, E. R. Markaryan, V. A. Maslov, N. K. Skobelev, and Yu. G. Sobolev, *Bull, Rus. Acad. Sci. Phys.* **70**, 1558 (2006).
- [11] C. Signorini, A. Yoshida, Y. Watanabe, D. Pierroutsakou, L. Stroe, T. Fukuda, M. Mazzocco, N. Fukuda, Y. Mizoi, M. Ishihara, H. Sakurai, A. Diaz-Torres, and K. Hagino, *Nucl. Phys. A* **735**, 329 (2004).
- [12] A. M. Vinodkumar, W. Loveland, R. Yanez, M. Leonard, L. Yao, P. Bricault, M. Dombsky, P. Kunz, J. Lassen, A. C. Morton, D. Ottewell, D. Preddy, and M. Trinczek, *Phys. Rev. C* **87**, 044603 (2013).
- [13] R. Raabe *et al.*, *Nature* **431**, 823 (2004).
- [14] A. Lemasson *et al.*, *Phys. Rev. Lett.* **103**, 232701 (2009).
- [15] M. Alcorta *et al.*, *Phys. Rev. Lett.* **106**, 172701 (2011).
- [16] L. Canto, P. Gomes, R. Donangelo and M. Hussein, *Phys. Rep.* **424**, 1 (2006).
- [17] L. Canto, P. Gomes, R. Donangelo, J. Lubian and M. Hussein, *Phys. Rep.* **596**, 1 (2015).
- [18] A. Diaz-Torres and I. J. Thompson, *Phys. Rev. C* **65**, 024606 (2002).
- [19] K. Hagino, A. Vitturi, C. H. Dasso and S. M. Lenzi, *Phys. Rev. C* **61**, 037602 (2000).
- [20] M. Ito, K. Yabana, T. Nakatsukasa, and M. Ueda, *Phys. Lett.* **B637**, 53 (2006).

- [21] G.F. Bertsch and H. Esbensen, Ann. Phys. (NY) **209**, 327 (1991).
- [22] H. Esbensen, G.F. Bertsch, and K. Hencken, Phys. Rev. C **56**, 3054 (1999).
- [23] K. Hagino and H. Sagawa, Phys. Rev. C **72**, 044321 (2005).
- [24] W. Loveland *et al.*, Phys. Rev. C **74**, 064609 (2006).
- [25] A. M. Vinodkumar, W. Loveland, P. H. Sprunger, L. Pristbrey, M. Trinczek, M. Dombsky, P. Machule, J. J. Kolata and A. Roberts, Phys. Rev. C **80**, 054609 (2009).
- [26] A. Chatterjee, A. Navin, A. Shrivastava, S. Bhattacharyya, M. Rejmund, N. Keeley, V. Nanal, J. Nyberg, R. G. Pillay, K. Ramachandran, I. Stefan, D. Bazin, D. Beaumel, Y. Blumenfeld, G. de France, D. Gupta, M. Labiche, A. Lemasson, R. Lemmon, R. Raabe, J. A. Scarpaci, C. Simenel, and C. Timis, Phys. Rev. Lett. **101**, 032701 (2008).
- [27] N. Rowley, in the proceedings of the International workshop on “Fusion Dynamics at the Extremes”, ed. by Yu. Ts. Oganessian and V.I. Zagrebaev (World Scientific, Singapore, 2001), p. 296.
- [28] K. Hagino, N. Rowley, and A. Kruppa, Comp. Phys. Comm. **123**, 143 (1999).
- [29] Ö. Akyüz and A. Winther, Proceedings of the Enrico Fermi School of Physics, 1979, (1981).
- [30] C. Dasso and G. Pollaro, Phys. Lett. B **155**, 223 (1985).
- [31] T. Furumoto, T. Suhara and N. Itagaki, Phys. Rev. C **87**, 064320 (2013).
- [32] N. Rowley, G. Satchler and P. Stelson, Phys. Lett. B **254**, 25 (1991).
- [33] Ki-Seok Choi, Myung-Ki Cheoun, K. S. Kim, T. H. Kim, and W. Y. So, J. Korean. Phys. Soc. **70**, 42 (2017).
- [34] N. Takigawa and H. Sagawa, Phys. Lett. B **265**, 23 (1991).
- [35] G. Bertsch, J. Borysowicz, H. McManus and W. Love Nucl. Phys. A **284**, 399 (1977); G. Satchler and W. Love Phys. Rep. **55**, 183 (1979); G. Satchler Nucl. Phys. A **329**, 233 (1979).
- [36] G. Satchler, Nucl. Phys. A **579**, 241 (1994).
- [37] W. Y. So, K. S. Kim, K. S. Choi and M. K. Cheoun, Phys. Rev. C **90**, 054615 (2014).
- [38] W. von Oertzen and I. Krouglov, Phys. Rev. C **53**, R1061(R) (1996).
- [39] V. I. Zagrebaev, Phys. Rev. C **67**, 061601(R) (2003).